Channel Capacities of Indoor MIMO-UWB Transmission for Different Material Partitions

Shu-Han Liao[1], Hua-Pin Chen[2], Chien-Ching Chiu[1]* and Chun-Liang Liu[1]

[1]*Department of Electrical Engineering, Tamkang University, Tamsui, Taiwan 251, R.O.C.*
[2]*Department of Electronic Engineering, Ming Chi University of Technology, Taishan, Taiwan 243, R.O.C.*

Abstract

In this paper, channel capacities of indoor MIMO-UWB (multiple input multiple output-Ultra wideband) transmission for different material partitions are described. A ray-tracing technique is applied to compute the frequency responses for an environment with different material partitions. All the material parameters of our simulation environments such as dielectric constant and conductivity are both dependent on operating frequency in our calculations for UWB transmission. In other words, these material parameters are frequency selective for our calculation. By frequency responses of our simulation environment, channel capacities of MIMO-UWB transmission are calculated. Furthermore, outage probability is also computed for analyzing statistical property. Based on the calculations, the effects by different material partitions on 2X2 MIMO-UWB transmission are compared for different signal power to noise power ratio (SNR). In addition, the effects by different material partitions for different antenna array are investigated and compared to SISO (single input single output). Numerical results show that the Styrofoam partition has largest transmission rate, and the plywood partition has smallest one. Finally, it is worth noting that in these cases the present work provided not only comparative information but also quantitative information.

Key Words: MIMO-UWB, Frequency Selective, Ray-Tracing Technique, Channel Capacity

1. Introduction

Channel capacity is an important parameter for wireless communication system. The parameter can be calculated by Shannon's theorem for a narrowband flat fading channel but it can't apply to a wideband frequency selective fading channel directly. In the general case, channel capacity of wideband frequency selective fading channel can consist of many channel capacities of narrowband flat fading at each discrete frequency point. UWB is a promising radio technique for wireless communication and it can deliver very high data rates for short ranges [1,2]. One of the reasons is that the bandwidth of UWB is very huge (from 3.1 to 10.6 GHz), which is allocated by Federal Communications Commission (FCC) [3]. Some studies about channel capacity of UWB have been researched and published [4–7].

Channel capacity of MIMO for wireless communications in a rich multi-path environment is larger than that offered by conventional techniques [8–12]. Channel capacity of UWB transmission or MIMO transmission has been discussed separately in many literatures. However, there are only few papers dealing with channel capacity of MIMO-UWB transmission. In the reference [13], they get channel capacity of MIMO-UWB transmission by measurement. That method is precise, however, it must cost a lot of time for measurement. In the reference [14], they calculate channel capacity by Saleh-Valenzuela (S-V) statistical approach. S-V statistical approach is a general multi-path channel model

*Corresponding author. E-mail: chiu@ee.tku.edu.tw

for UWB transmission. It can be used to simulate four different scenes, including line of sight (LOS) and non LOS [15]. However, S-V statistical approach is not enough for more realistic environments compared to ray-tracing model. Some literatures using ray-tracing technique about UWB [16–18] or MIMO [19–21] have been published.

Since UWB can support very high data rates, and MIMO can be used to increase channel capacity and transmission quality. Combination of the two techniques is a good choice in indoor transmission. In this paper, we use a ray-tracing technique, which can promise the computing time and reality in environment, to calculate channel frequency responses of MIMO-UWB transmission for different material partitions. The effects of different materials of partitions with brick block, concrete block, drywall, close office partition, plywood, structure wood and styrofoam on the MIMO-UWB communication characteristics are presented. All the material parameters of our simulation environments such as dielectric constant and conductivity are both dependent on operating frequency in our calculations for UWB transmission. All the values of dielectric constant and conductivity of these partitions versus operating frequency can refer to reference [22]. By frequency responses of our simulation environment, channel capacities of MIMO-UWB transmission are calculated. Furthermore, outage probability is also computed for analyzing statistical property. Based on the calculations, the effects by different material partitions on 2X2 MIMO-UWB transmission are compared for different SNR. In addition, the effects by different material partitions for different antenna array are investigated and compared to SISO. The rest of this paper is organized as follows. Section 2 introduces the channel modeling by ray-tracing technique. In section 3, we calculate channel capacity and outage probability for MIMO-UWB transmission. Section 4 presents our simulation architecture and numerical results. Some conclusions are drawn in section 5.

2. Channel Modeling

A ray-tracing technique is a good technique to calculate channel frequency response for wireless communication [16–21]. As a result, we develop a ray-tracing technique to model channel for our simulations. Using ray-tracing techniques to predict channel characteristic is effective and fast [23–25]. Thus, a ray-tracing channel model is developed to calculate the channel matrix of UWB system. Flow chart of the ray-tracing process is shown in Figure 1. It conceptually assumes that many triangular ray tubes (not rays) are shot from a transmitter. Here the triangular ray tubes whose vertexes are on a sphere are determined by the following method. Fist, we construct an icosahedron which is made of 20 identical equilateral triangles. Then, each triangle of the icosahedron is tessellated into a lot of smaller equilateral triangles. Finally, these small triangles are projected on to the sphere and each ray tube whose vertexes are determined by the small equilateral triangle is constructed.

For each ray tube bouncing and penetrating in the environments, we check whether reflection times and penetration times of the ray tube are larger than the numbers of maximum reflection N_{ref} and maximum penetration N_{pen}, respectively. If it does not, we check whether the receiver falls within the reflected ray tube. If it does, the contribution of the ray tube to the receiver can be attributed to an equivalent source (image). In other words, a specular ray going to receiver exists in this tube and this ray can be thought as launched from an image source. Moreover, the field diffracted from illuminated wedges of the objects in the environment is calculated by uniform theory of diffraction (UTD) [26]. Note that only first diffraction is considered in this paper, because the contribution of second diffraction is very small in the analysis. As a result, the corresponding equivalent source (image) can be determined. Some details can refer to literature [27]. By using these images and received fields, the channel frequency response can be obtained as follows

$$H(f) = \sum_{p=1}^{N_p} a_p(f) e^{j\theta_p(f)} \tag{1}$$

where p is the path index, N_p is the total numbers of path, f is the frequency of sinusoidal wave, $\theta_p(f)$ is the pth phase shift and $a_p(f)$ is the pth receiving magnitude. And channel frequency response of UWB can be calculated by equation (1) in the frequency range of UWB.

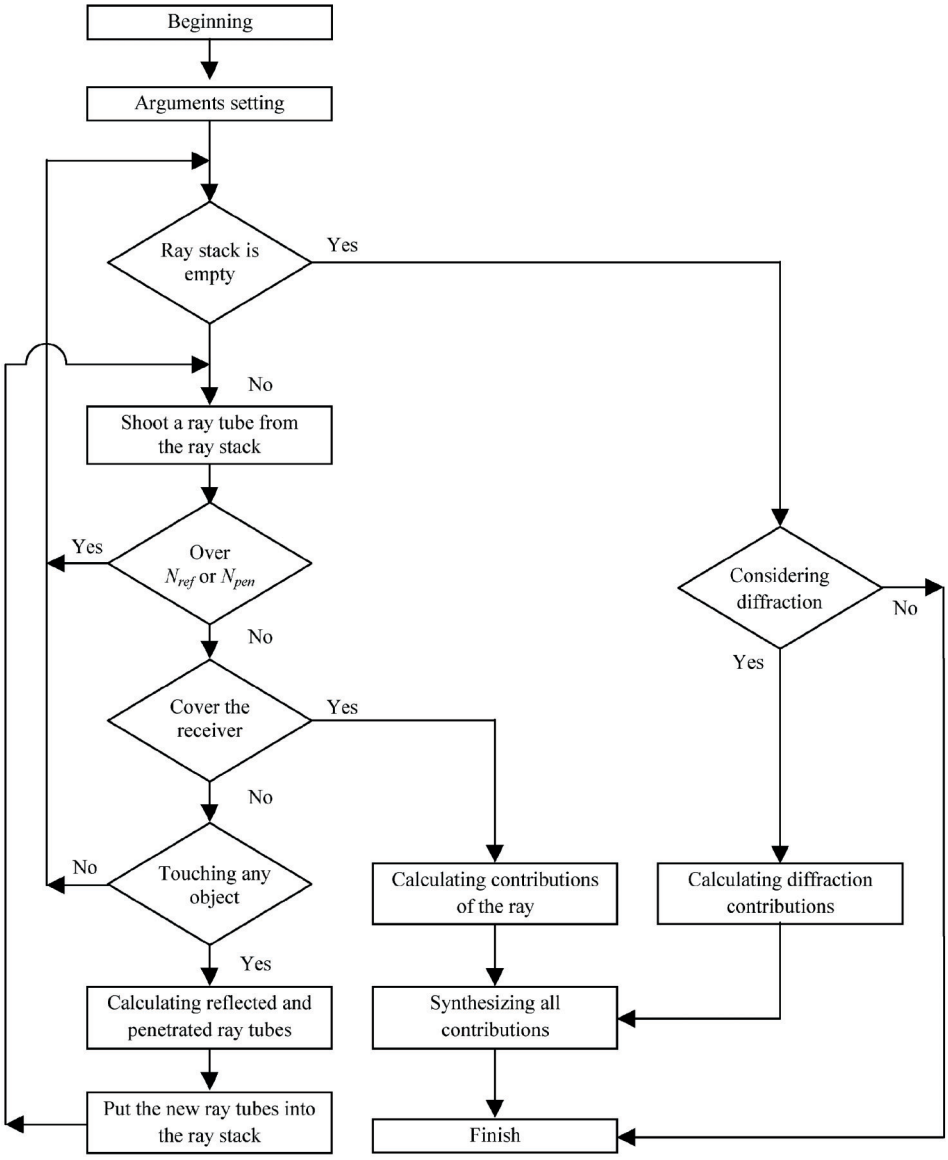

Figure 1. Flow chart of the ray-tracing process.

3. Calculations of Channel Capacity and Outage Probability

3.1 MIMO Channel Capacity of Narrowband Transmission

A narrowband time-invariant wireless channel with n_t transmitter and n_r receiver antennas can be described by an n_r by n_t deterministic matrix H. The received signal is described by

$$Y = HX + W \tag{2}$$

where $Y \in \Re^{n_r}$, $X \in \Re^{n_t}$ and $W \in \Re^{n_r}$ denote the received signal, transmitted signal and zero mean additive white Gaussian noise at a symbol time, respectively.

The capacity of the matrix H can be computed by decomposing the channel into a set of parallel and independent scalar Gaussian sub-channels by basic linear algebra. The matrix H can be expressed by singular value decomposition (SVD)

$$H = E\Lambda F^{*} \tag{3}$$

where $E \in \Re^{n_r \times n_r}$ and $F^{*} \in \Re^{n_t \times n_t}$ are unitary matrix. $\Lambda \in \Re^{n_r \times n_t}$ is a rectangular matrix whose diagonal elements are non-negative real values and other elements are zero.

A MIMO system is capable of signal processing at the transmitter and receiver to produce the set of received signals with highest overall capacity. If we define

$$X = F\hat{X} \tag{4}$$

$$\hat{Y} = E^{*}Y \tag{5}$$

$$\hat{W} = E^{*}W \tag{6}$$

then we can rewrite the equation (2) as

$$\hat{Y} = \Lambda\hat{X} + \hat{W} \tag{7}$$

Because the unitary matrices don't change the geometrical length of vectors, so we don't add any power to the total transmitted signal. Thus, the energy is preserved and we have an equivalent representation as a parallel Gaussian channel

$$\hat{y}_i = \lambda_i \times \hat{x}_i + \hat{w}_i \qquad i = 1,2,...,n_{\min} \tag{8}$$

where $n_{\min} := \min(n_t, n_r)$, $\hat{y}_i$, λ_i, $\hat{x}_i$ and $\hat{w}_i$ are the ith diagonal element corresponded to the matrix $\hat{Y}$, Λ, $\hat{X}$ and $\hat{W}$, respectively. The equivalent architecture of MIMO system is plotted in Figure 2.

Now, the MIMO channel capacity of narrowband transmission can be expressed as

$$C^{narrowband} = W\sum_{i-1}^{n_{\min}} \log_2\left(1 + \frac{\lambda_i^{\,2} P_i}{N_o W}\right) \quad \text{(bits/sec/Hz)} \tag{9}$$

where P_i is the transmitting power for the ith sub-channel, N_o is power spectrum density of AWGN and W is the bandwidth of the narrowband channel. If we assume that the transmitter has excited each separate channel with equal power, then the equation (9) can be rewritten as

$$C^{narrowband} = W\sum_{i=1}^{n_{\min}} \log_2\left(1 + \lambda_i^{\,2} \times \frac{SNR_t}{n_{\min}}\right) \quad \text{(bits/sec/Hz)} \tag{10}$$

where SNR_t is the total transmitting power to noise power ratio. Note that the equation (10) is similar to most channel capacity of MIMO system [8–12].

3.2 MIMO Channel Capacity of UWB Transmission

An $N_t \times N_r$ UWB system is represented by the three-dimensional matrix $\mathrm{H}^{UWB} \in C^{N_r \times N_t \times N_f}$ such that $\mathrm{H}^{UWB} = [\mathrm{H}_f^{narrowband}], f = 1, 2, ..., N_f$, where $\mathrm{H}_f^{narrowband}$ is defined as a flat-fading channel matrix of MIMO narrowband system at the fth frequency component and N_f is the number of discrete frequency components of UWB system. When the frequency components of a wideband channel are uncorrelated to each other, it is possible to divide the wideband channel into several narrowband channels. As a result, MIMO capacity of UWB systems can be seen as the

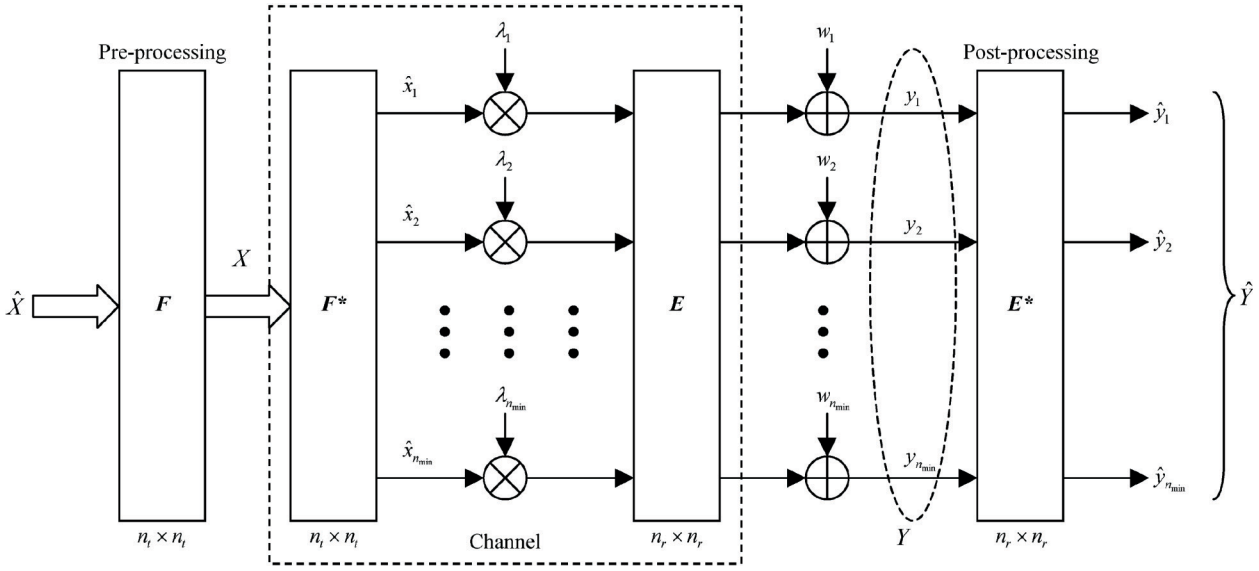

Figure 2. Equivalent architecture of MIMO system through the SVD.

summation of several MIMO capacities of narrowband systems at every discrete frequency component.

By the ray-tracing technique, all the frequency responses inside the bandwidth of UWB between any transmitter and receiver antennas are calculated. Then, MIMO channel capacity of UWB transmission can be calculated as summation of many channel capacities of narrowband at each discrete frequency point. Thus, the channel capacity (bandwidth efficiency) can be written as

$$C^{UWB} = \frac{1}{BW}\sum_{f=1}^{N_f} C_f^{narrowband} \quad \text{(bits/sec/Hz)} \tag{11}$$

where $C_f^{narrowband}$ is the MIMO capacity of narrowband systems at the fth frequency component, BW is the total bandwidth of UWB and N_f are the numbers of frequency components.

3.3 Outage Probability

In the practical communication systems, it is important to investigate the channel capacity in the sense of outage probability. An outage probability is defined as the event that the communication channel does not support a target data rate. If we give a data rate R, then the outage probability can be written as

$$P_o = P\{C^{UWB} < R\} \tag{12}$$

Based on the above discussion, we can calculate the channel capacity and outage probability of MIMO-UWB transmission in indoor environment.

4. Simulation versus Time Domain Measurements

In the present work, the results of ultra wideband time domain measurement in the laboratory (Lab) environment are presented.

4.1 Measurement Setup

A diagram of the time domain measurement setup is shown in Figure 3. At the transmitter side, a pulse generator was used as an UWB signal source. The width of the transmitting pulse is duration about 30 *ps*. This generator was connected to the transmitting antenna through a low loss wideband cable. The output signal of the receiving antenna was amplified by a low noise amplifier. A digital sampling oscilloscope was used at the receiver side which sampled the received signal at a rate of 1 sample per 25 *ps*. The pulse generator and the digital sampling oscilloscope were synchronized through a reference clock signal. Measurements were performed by a pair of 1–26 GHz horn antenna. These transmitting and receiving antennas were both placed at a height of 1.5 m above ground.

4.2 Measurement Location

The time domain measurement campaign was conducted for line of site (LOS) scenarios at the microwave Lab. Figure 4 is the Microwave laboratory in Tamkang University and this laboratory has dimensions of 9.2 m (Length) × 10 m (Width) × 3 m (Height). The building walls are made of concrete block. The partitions are wood structured. The doors are made of wood. The Lab envi-

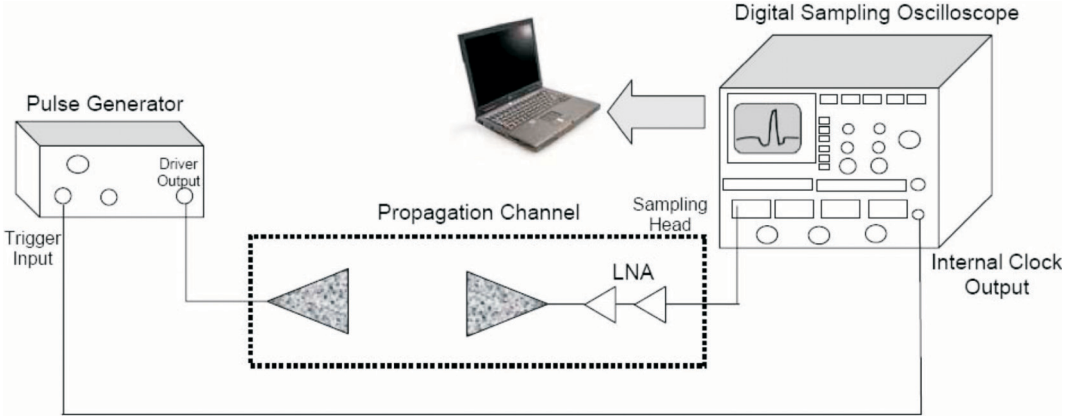

Figure 3. A diagram of the time domain measurement system.

ronments are equipped with many electronic and measurement devices which are located on tables. Most of these devices are made of metallic materials. The transmitting antenna Tx and receiver antenna Rx are plotted in Figure 4. The transmitting and receiving antennas are UWB antenna. The transmitting antenna Tx (7.43, 3.75, 1.5) m is located on the center of the right area in the Microwave laboratory. The receiver antenna Rx (7.43, 1.45, 1.5) m in the laboratory are chosen for simulations and measurement.

4.3 Measurement Procedure

To perform the measurements, receiver points were chosen at locations Rx where the received signal could be clearly detected. The measurements were collected received signal by receiver antenna. The received signal of the proposed antenna is shown in Figure 5(a). In the simulations, external noise in the channel propagation has been considered. The received signal $r(t)$ can be expressed as follows:

$$r(t) = [x(t) \otimes h_b(t)] + n(t) \tag{13}$$

where $x(t)$ is the transmitted UWB pulse signal and $h_b(t)$ is the impulse response of the channel, $n(t)$ is the white Gaussian noise with zero mean and variance $N_0/2$. The simulated received signal is shown in Figure 5(b). Simulation results show that the received signal in Figure 5(a) quite matches to that in Figure 5(b) in the received signal.

Two different room layouts for the indoor MIMO-UWB channel measurement in reference [28] are shown in Figures 6 and 7 respectively. The two rooms contain wooden benches, wooden doors and metallic cabinets with various sizes, and the walls, ceilings and the grounds are made of concrete block. Furthermore, both LOS and non-LOS (NLOS) scenarios are considered in the two rooms, while LOS blockage is created by placing a perfect electric conductor (PEC) board.

The antennas of both transmitter and receiver are at a height of 1.5 m from the ground with omni-directional radiation. Furthermore, The Rx grid having a 1 m^2 horizontal region is used to get statistically reliable data, and the grid places the receiving antenna at 11 consecutive

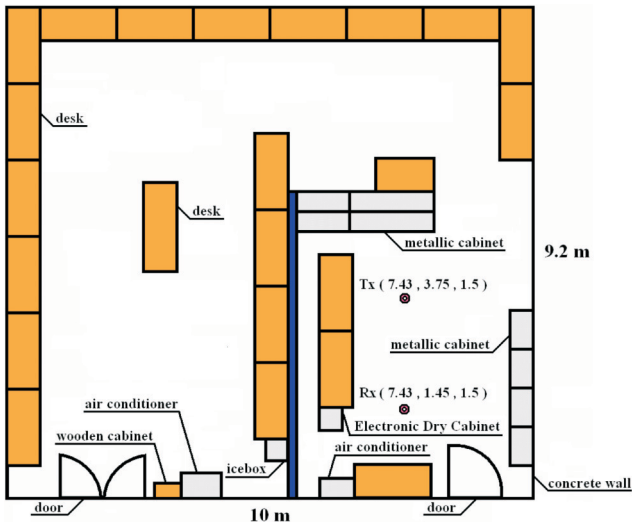

Figure 4. Dimensions and geometry of the microwave Lab (housed within the department of electronic engineering, Tamkang, University of Taiwan. The height of microwave lab is 3 meters).

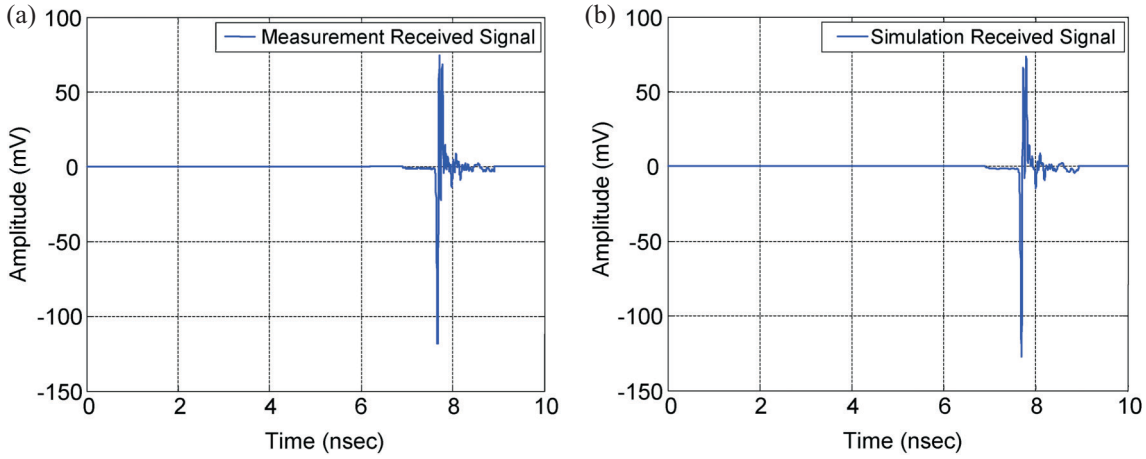

Figure 5. The received signal at Rx (a) measurement (b) simulation.

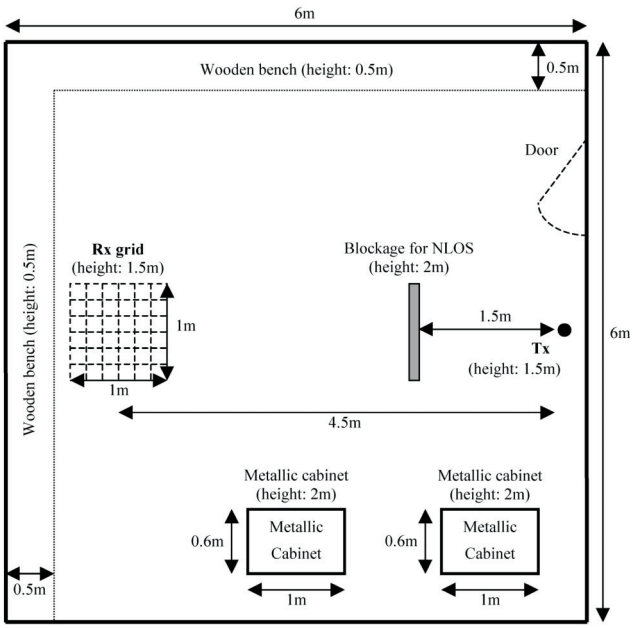

Figure 6. Layout of the indoor MIMO-UWB channel measurement in the first room.

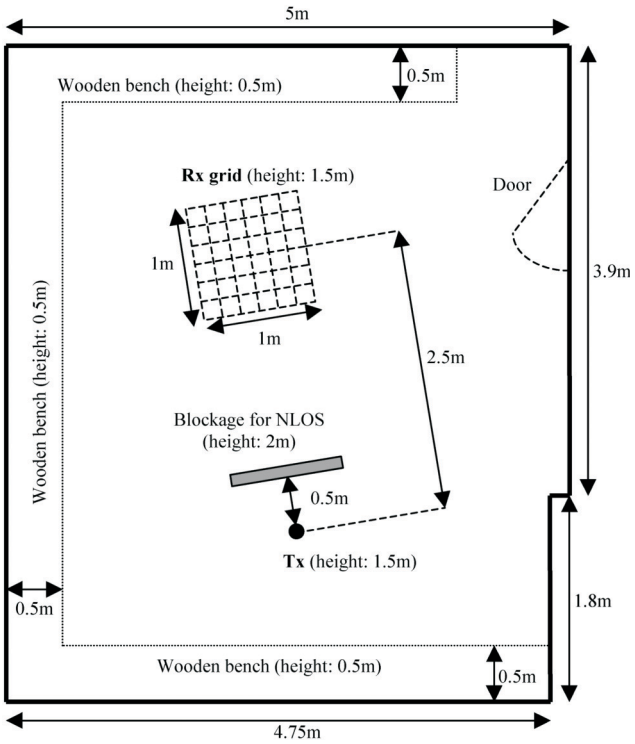

Figure 7. Layout of the indoor MIMO-UWB channel measurement in the second room.

positions at 0.1 m separation. In this manner, 121 individual MIMO-UWB channel matrices are obtained in each environment. The channel realizations for various receiving locations are combined into one ensemble with 121 samples, and such data sets are obtained for both LOS and NLOS scenarios.

In the simulation, the channel is assumed to have N_f = 1601 discrete frequency points over the BW = 7.5 GHz wideband from f_l = 3.1 GHz to f_H = 10.6 GHz with $\Delta f \approx$ 4.7 MHz resolution. The inter-element separation d = 0.06 m is chosen in order to achieve low spatial correlation [29], while the largest wavelength is $\lambda_l = c/f_l \approx 0.1$ m, where $c = 3 \times 10^8$ m/s is the speed of light. Furthermore, channel capacity calculated is based on normalized the channel matrix. Normalization process separates the problems of calculating link-budget power and of studying the effects of channel fading. Finally, note that strict time stationary is maintained by ensuring complete physical isolation and absence of any mobile objects.

Based on the same environmental frameworks and measurement conditions, channel capacity of MIMO-UWB system is calculated by the modified ray-tracing channel model. Cumulative distribution functions (CDFs) of the channel capacities calculated by the channel model for different array sizes at SNR = 10 dB are shown in Figures 8 and 9 for LOS and NLOS scenarios, respectively. In Figure 8, the curve for 1X3 array is close to that for 2X2 array, since specular reflection, penetration and edge diffraction can not provide sufficient scattering except the contribution of LOS signal in the environment. That is, the channel capacities for the two antenna arrays are similar at SNR = 10 dB in the environment. For NLOS scenario, because the contribution of LOS signal has removed, more ideal scattering phenomenon exists in the environment. In other words, the spatial correlation between the sub-channels becomes less. As a result, the channel capacity calculated from some simulation locations for 2X2 array will be larger than that for 1X3 array, and that is why the curve for 2X2 array separates from the curve for 1X3 array in Figure 9.

First-order statistics of the channel capacities for different array sizes at SNR = 10 dB, calculated by the channel model, are listed in Table 1(a), while that given in reference [28] are listed in Table 1(b). Compared the two tables, the ergodic capacity for different antenna array sizes calculated by the channel model reasonably match that given in [28]. Note that some scattering objects are not built in the simulation environments for the channel model, because the positions and sizes of these objects

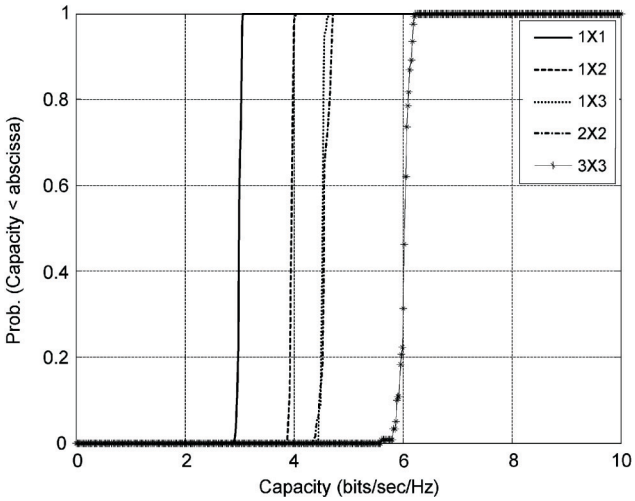

Figure 8. CDFs of the channel capacities obtained by the modified ray-tracing channel model for different array sizes at *SNR* = 10 dB for LOS scenario.

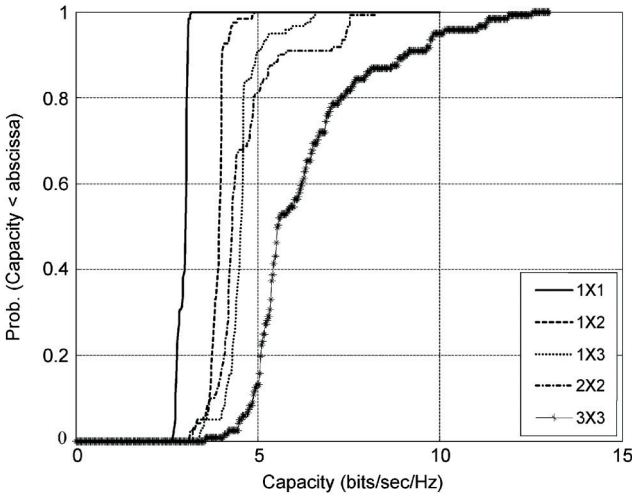

Figure 9. CDFs of the channel capacities obtained by the modified ray-tracing channel model for different array sizes at *SNR* = 10 dB for NLOS scenario.

Table 1(a). First-order statistics of the channel capacities for different array sizes at *SNR* = 10 dB, calculated by the modified ray-tracing channel model

Array size	Line-of-sight (LOS)			Non-line-of-sight (NLOS)		
	1% outage	Ergodic	Std. Dev.[1]	1% outage	Ergodic	Std. Dev.
1X1	2.9	2.9	0.1	2.7	2.9	0.2
1X2	3.9	3.9	0.1	3.2	3.9	0.2
1X3	4.5	4.5	0.1	3.4	4.5	0.4
2X2	4.4	4.5	0.2	3.1	4.7	0.8
3X3	5.8	5.9	0.2	4.0	6.4	1.3

Table 1(b). First-order statistics of the channel capacities for different array sizes at *SNR* = 10 dB, given in [28]

Array size	Line-of-sight (LOS)			Non-line-of-sight (NLOS)		
	1% outage	Ergodic	Std. Dev.	1% outage	Ergodic	Std. Dev.
1X1	2.3	2.6	0.1	2.5	2.6	0.1
1X2	3.3	3.6	0.1	3.4	3.7	0.1
1X3	3.9	4.2	0.1	4.0	4.3	0.1
2X2	4.3	4.7	0.2	4.4	4.8	0.2
3X3	6.2	6.8	0.3	6.3	7.0	0.3

Table 1(c). First-order statistics of the channel capacities for different array sizes at SNR = 10 dB, calculated by the modified S-V channel model

Array size	Line-of-sight (LOS)			Non-line-of-sight (NLOS)		
	1% outage	Ergodic	Std. Dev.	1% outage	Ergodic	Std. Dev.
1X1	2.8	2.9	0.1	2.8	2.9	0.1
1X2	3.2	4.2	0.7	3.2	4.2	0.7
1X3	3.2	4.8	0.8	3.3	4.9	0.8
2X2	3.4	5.8	1.3	3.4	5.9	1.3
3X3	4.4	8.8	2.1	4.8	9.0	2.3

[1] Std. Dev. means standard deviation.

are not clearly described in [28]. In other words, the scattering diverseness for the simulation is less than that for measurement. As a result, few differences of the first-order statistics of the channel capacity between the channel model and the measurement can be seen in the table. It is well-known that a system which provides more spatial degree of freedom is more sensitive to environmental complication (i.e., scattering diverseness). As a result, the difference of the ergodic capacity between the channel model and the measurement for 3X3 array is larger than that for 2X2 array. Furthermore, for LOS scenario, the 1% outage capacities is as similar as ergodic capacities for all antenna array sizes, since the scattering diverseness is not enough except the contribution of LOS signal for the channel model. In other words, the channel capacities for all simulation position are similar. The same reason can explain that the standard deviations of the channel capacities for all antenna sizes are small and that is why all the curves are very sharp in Figure 8. In contrast to LOS scenario, NLOS scenario expresses the more scattering diverseness exist in the environment. As a result, the 1% outage capacities are smaller than ergodic capacities, and the standard deviations of the channel capacities become large, for all antenna array sizes. The same reason can explain why all the curves are flat in Figure 9. Note that the differences become significant when the antenna size becomes large. It is concluded that the channel model can obtain precise channel capacity in the specific environment.

Channel capacities of UWB systems with SIMO and MIMO are also calculated by the modified S-V channel model. The calculating results calculated by the channel model are also compared with that given in reference [28]. CM1 channel is made for LOS scenario and CM2 channel is made for NLOS scenario, and 242 channel realizations are chosen for both the scenarios. Note that the channel model can not adjust arbitrarily the parameters which affect spatial component such as antenna spacing, antenna polarization and antenna position, etc. However, the channel model which records a lot of experimental results can provide the statistical numerical results for four different scenarios.

CDFs of the channel capacities calculated by the channel model for different array sizes at *SNR* = 10 dB are shown in Figures 10 and 11 for LOS and NLOS scenarios, respectively. Since the modified S-V model is a statistical model based on various measurements in the more than 400 environments with rich scattering, the capacities of MIMO are always higher than that of SIMO for both LOS and NLOS scenarios, and all the standard deviations of the channel capacities for all antenna sizes are large. As a result, all the curves created by the channel model are flatter than that created by the modified ray-tracing channel model. The first-order statistics of channel capacity calculated by the channel model at *SNR* = 10 dB are listed in Table 1(c).

The first-order statistics of channel capacity calculated by the channel model at *SNR* = 10 dB are listed in

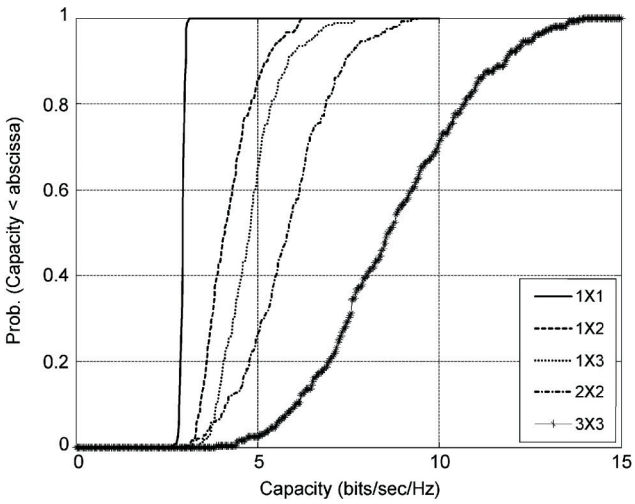

Figure 10. CDFs of the channel capacities obtained by the modified S-V channel model for different array sizes at *SNR* = 10 dB for LOS scenario.

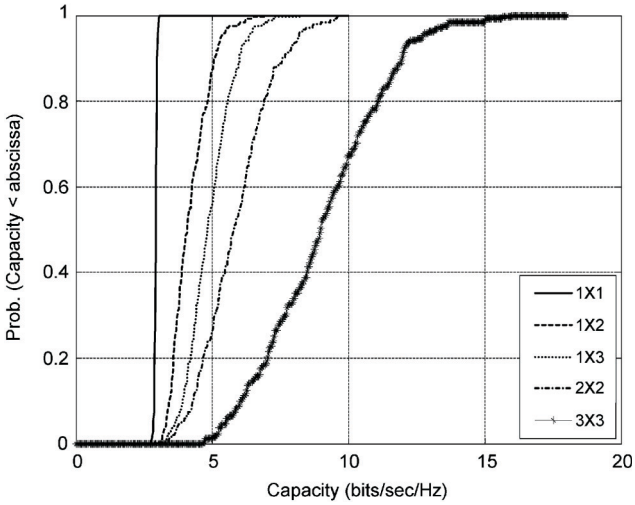

Figure 11. CDFs of the channel capacities obtained by the modified S-V channel model for different array sizes at *SNR* = 10 dB for NLOS scenario.

Table 1(c). In contrast to Table 1(b), Table 1(c) shows that the corresponding ergodic capacities and standard deviations are higher, and the corresponding 1% outage capacities are lower, for all antenna array sizes. Furthermore, in Table 1, it is seen the differences between Table 1(b) and Table 1(c) are larger than that between Table 1(b) and Table 1(a). The major reason is that the simulation conditions for the S-V channel model can not match the measurement conditions provided by the reference. It is concluded that the S-V channel model can only provide a rough statistic of channel capacity.

The first-order statistic of channel capacities of UWB systems with different antenna array sizes have been calculated by the modified ray-tracing channel model and the modified S-V channel model, and the numerical results calculated by the two channel models are compared with that provided by the reference. The modified S-V channel model can provide a rough statistic of channel capacity, but it is not precise to be applied in the specific environment. In other words, the statistical numerical results can not be always instead of the deterministic numerical results in the specific environment, since the statistical numerical results are calculated based on various measurements in the more than 400 environments with rich scattering, implying the numerical results in the specific environment is very different to that calculated by the channel model. However, the modified S-V channel model can save much processing time.

In contrast to the modified S-V channel model, the modified ray-tracing channel model provides more adjustable parameter to calculate channel capacity of MIMO-UWB system for obtaining more precise results. Numerical results show that the numerical results created by the channel model are as similar as that by the measurement provided by the reference [28]. As a result, the channel model can be used in place of measurement in the specific environment.

In conclusion, the two channel models can not only resolve the drawbacks caused by the measurement but also keep good accuracy for individual necessary. In other words, the modified S-V channel model can provide rough statistic of channel capacity and save much processing time compared to the modified ray-tracing channel model, and the modified ray-tracing channel model can provide precise channel capacity in the specific environment.

5. Numerical Results

In this section, the channel capacities and outage probabilities of MIMO-UWB transmission for different material partitions are computed by the section 2 and section 3. We build an environment and then calculate the frequency responses between each transmitter and each receiver. The frequency responses from 3 GHz to 10 GHz with step 5 MHz are calculated for satisfying the bandwidth of UWB. The top view of our simulation environment is shown in Figure 12. In Figure 12, there are two adjacent rooms in our simulation environment, which has a partition between them. The dimensions of the two rooms are both 5.5 m (length) × 5.5 m (width) × 3 m (height). The partition has dimensions of 5.5 m (length) × 0.2 m (thickness) × 3 m (height). All the materials of objects in our simulation are chosen to concrete block except the partition. Furthermore, seven different material partitions are considered, including brick block, concrete block, drywall, close office partition, plywood, structure wood and Styrofoam. The dielectric constants and conductivities of the seven material partitions are both dependent on operating frequency for UWB transmission. For example, the dielectric constants and conductivities of the concrete block and Styrofoam for different frequency are shown in Table 2. These parameters of other material partitions can refer to reference [22].

The transmitter Tx (2.75 m, 2.75 m, 0.8 m) is located in the center of the Room A. We choose one hundred receivers located in the Room B with uniform distribution and these receivers are characterize the statistical channel properties in our simulation environment. In other words, there are just little effects for statistical channel properties if we set more receivers in Room B. All the antenna heights of these receivers are chosen to 0.8 meters. In addition, different antenna arrays are also shown in Figure 12, including 2 × 2, 3 × 3 and 4 × 4. The space between adjacent antennas is 0.15 m for each antenna array, which satisfies minimum space ($\lambda_{max}/2$) without interference between adjacent antennas. Note that the maximum wavelength (λ_{max}) is 0.1 m in our simulation. Furthermore, the polarizations of both transmitting and receiving antennas are vertical.

In the first case, we compare the effects of seven material partitions on 2 × 2 MIMO-UWB transmission with different SNR_t. The numerical results are shown in Fig-

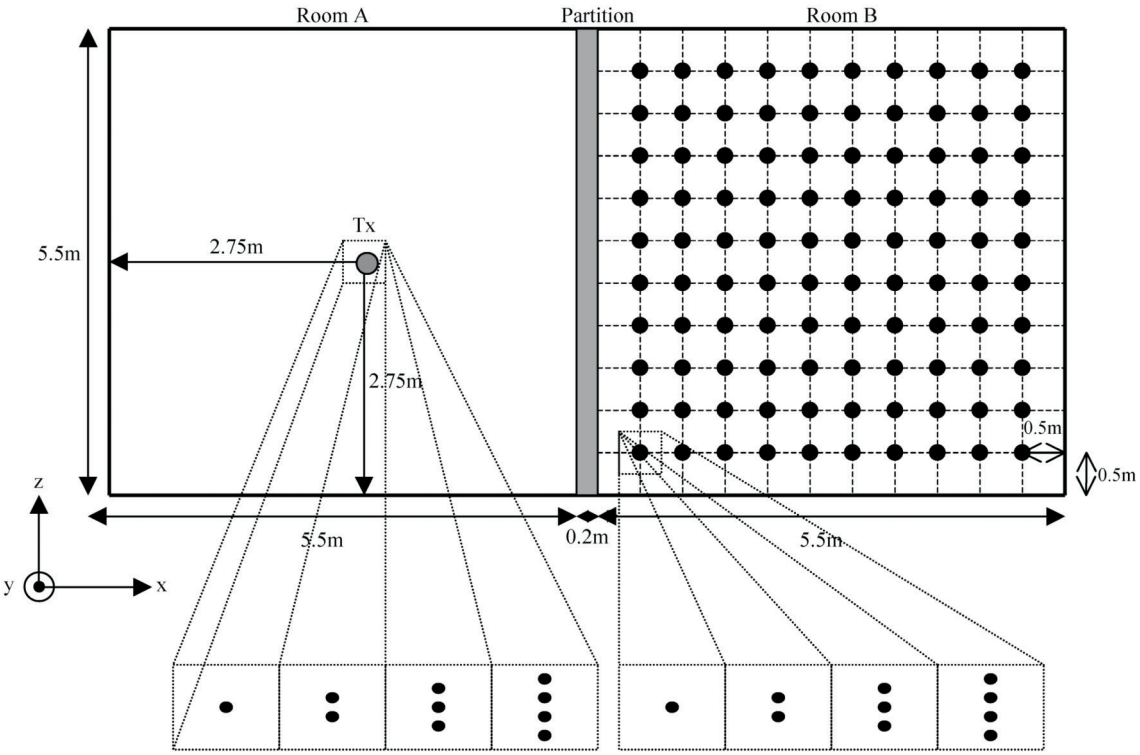

Figure 12. Top view of our simulation environment.

Table 2. The dielectric constants and conductivities of concrete block and Styrofoam for different frequency

Frequency (GHz)	Concrete block		Styrofoam	
	Dielectric constants ε_r	Conductivities $\sigma(s/m)$	Dielectric constants ε_r	Conductivities $\sigma(s/m)$
3.0	2.2500	6.56×10^{-2}	1.1300	1.88×10^{-4}
3.5	2.2750	6.64×10^{-2}	1.1300	2.20×10^{-4}
4.0	2.3000	6.39×10^{-2}	1.1300	2.51×10^{-4}
4.5	2.3150	6.51×10^{-2}	1.1300	2.83×10^{-4}
5.0	2.3300	6.47×10^{-2}	1.1300	3.14×10^{-4}
5.5	2.3150	6.64×10^{-2}	1.1300	3.45×10^{-4}
6.0	2.3000	6.71×10^{-2}	1.1300	3.77×10^{-4}
6.5	2.2750	6.68×10^{-2}	1.1300	4.08×10^{-4}
7.0	2.2500	6.56×10^{-2}	1.1300	4.39×10^{-4}
7.5	2.2750	6.73×10^{-2}	1.1300	4.71×10^{-4}
8.0	2.3000	6.85×10^{-2}	1.1300	5.02×10^{-4}
8.5	2.3150	6.89×10^{-2}	1.1300	5.34×10^{-4}
9.0	2.3300	6.87×10^{-2}	1.1300	5.65×10^{-4}
9.5	2.3150	6.66×10^{-2}	1.1300	5.96×10^{-4}
10.0	2.3000	6.39×10^{-2}	1.1300	6.28×10^{-4}

ures 13–15, which SNR_t is 35 dB, 40 dB and 45 dB, respectively. Note that the average SNR_r (receiving signal power to noise power ratio) is SNR_t subtracting about 25 dB in our cases and the value is about 10 dB, 15 dB and 20 dB, respectively. In these figures, it is found that the transmission rate increases when SNR_t increases for all the material partitions. The results can also be verified from equation (10). Furthermore, we can find that the materials of partitions corresponding to the transmission rate at any outage probability from high to low are Styro-

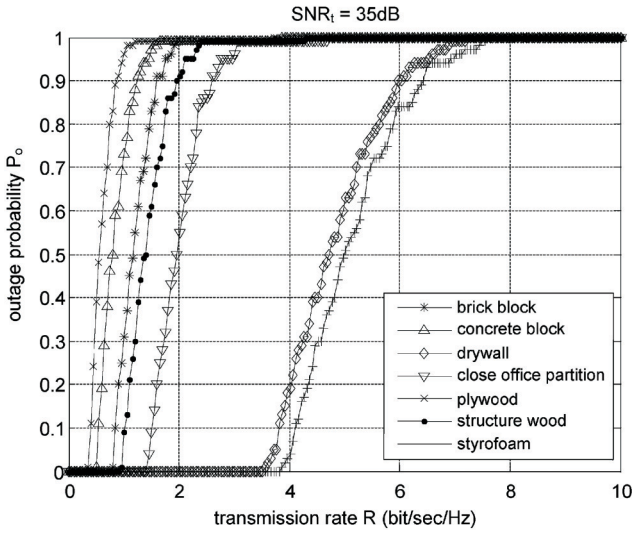

Figure 13. Outage probability versus transmission rate for seven material partitions on 2X2 MIMO-UWB system when the SNR_t is 35 dB.

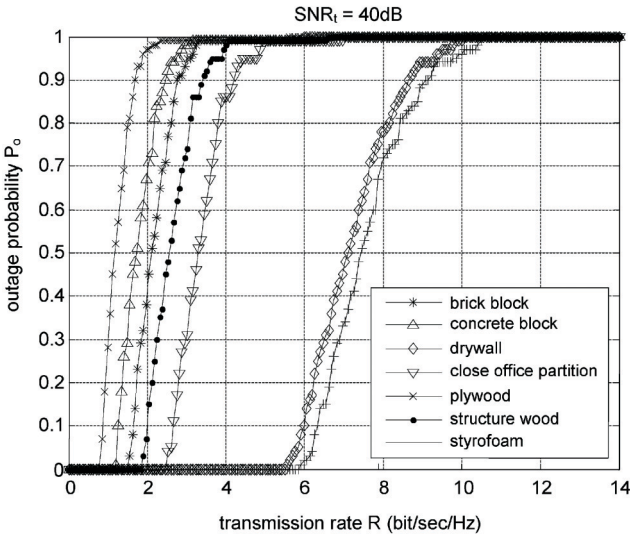

Figure 14. Outage probability versus transmission rate for seven material partitions on 2X2 MIMO-UWB system when the SNR_t is 40 dB.

foam, drywall, close office partition, structure wood, brick block, concrete block and plywood with each SNR_t. In other words, the Styrofoam partition has largest transmission rate, and the plywood partition has smallest one. The phenomenon can also be observed from the conductivities of these materials. The conductivities of Styrofoam and drywall are smaller than these for the others so that the propagation losses are lower than these for the others. Furthermore, we define a parameter R_m for determining criterion, which is the maximum transmission rate of MIMO-UWB transmission when outage probability is zero. Based on the criterion, the maximum transmission rates R_m for the seven material partitions are listed in Table 3. It is seen for example, the differences of R_m between Styrofoam and plywood are about 3.52, 5.07 and 6.87, which corresponds SNR_t to be 35 dB, 40 dB and 45 dB, respectively.

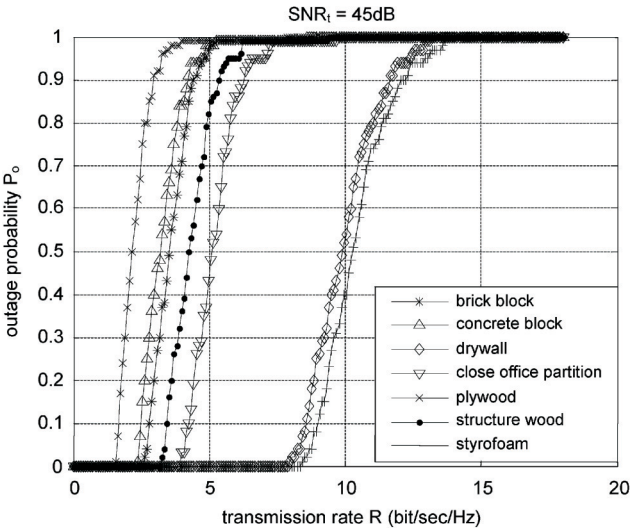

Figure 15. Outage probability versus transmission rate for seven material partitions on 2X2 MIMO-UWB system when the SNR_t is 45 dB.

Table 3. The maximum transmission rate for seven material partitions on 2X2 MIMO system for different SNR_t when the outage probability is zero

Materials	Maximum transmission rate R_m (bits/sec/Hz)		
	SNR$_t$ = 35 dB	SNR$_t$ = 40 dB	SNR$_t$ = 45 dB
brick block	0.75	1.48	2.53
concrete block	0.45	1.13	2.26
drywall	3.52	5.49	7.87
close office partition	1.41	2.46	3.89
plywood	0.30	0.77	1.45
structure wood	0.90	1.83	3.17
Styrofoam	3.82	5.84	8.32

In the second case, the effects of seven material partitions for different antenna array, including 2 × 2, 3 × 3 and 4 × 4 are compared to SISO when SNR_t is 45 dB. For example, the numerical results are shown in Figures 16, 17 and 18 for concrete block partition, plywood partition and Styrofoam partition, respectively. In these figures, it is found that the transmission rate compared to SISO will become large when the number of antenna array increases for all the materials of partitions at any outage probability. Furthermore, the values of transmission rate normalized to SISO for all the material partitions are similar when system is changed from SISO to MIMO. These values are about 1.58, 2.24 and 2.93 for 2 × 2 MIMO, 3 × 3 MIMO and 4 × 4 MIMO, respectively. In addition, the values of transmission rate normalized to SISO are not multiple of SISO because there are some correlations between MIMO antennas in the system. The maximum transmission rates R_m for the seven material partitions by different antenna array are listed in the Table 4.

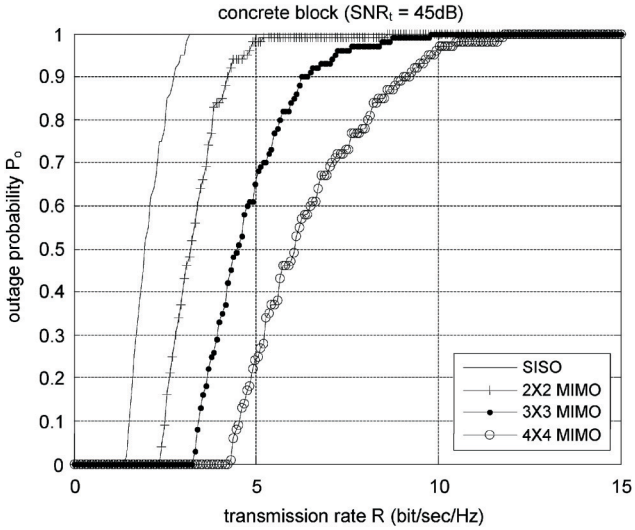

Figure 16. Outage probability versus transmission rate for concrete block partition by different antenna pair when the SNR_t is 45 dB.

6. Conclusion

A method for analyzing and calculating the channel capacity and outage probability for different material partitions and different antenna array in indoor MIMO UWB communication system has been presented. A realistic environment is built by a ray-tracing technique in this paper. Moreover, the parameters of all the materials in our simulations are considered to depend on operating frequency. i.e., the dielectric constant and conductivity of objects are not assumed to be frequency independent.

Numerical results show that the Styrofoam partition has largest transmission rate, and the plywood partition has smallest one. It is also seen that the transmission rate increases when SNR_t increases for all the materials of partitions. Furthermore, it is found that the transmission rate compared to SISO will become large when number of antenna array increases for all the material partitions

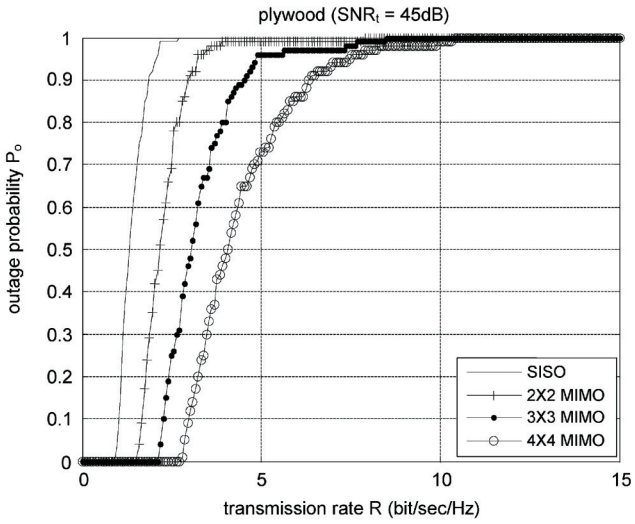

Figure 17. Outage probability versus transmission rate for plywood partition by different antenna pair when the SNR_t is 45 dB.

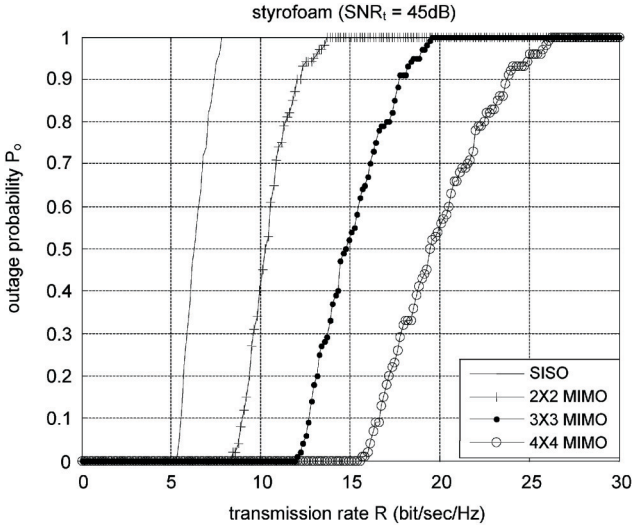

Figure 18. Outage probability versus transmission rate for Styrofoam partition by different antenna pair when the SNR_t is 45 dB.

Table 4. The maximum transmission rate for seven materials partitions by different antenna array with SNR_t = 45 dB when the outage probability is zero

Materials	Maximum transmission rate R_m (bits/sec/Hz)			
	SISO	2X2 MIMO	3X3 MIMO	4X4 MIMO
brick block	1.66	2.53	3.54	4.67
concrete block	1.36	2.26	3.24	4.22
drywall	5.13	7.87	11.31	14.77
close office partition	2.51	3.89	5.43	7.14
plywood	0.90	1.45	2.11	2.71
structure wood	2.01	3.17	4.42	5.83
Styrofoam	5.28	8.32	11.91	15.53

at any outage probability. Furthermore, the values of transmission rate normalized to SISO for all the material partitions are similar when system is changed from SISO to MIMO.

As a result, our research provides a method to calculate channel capacity and outage probability of MIMO-UWB transmission in indoor environment. These calculation can be used to determine the transmission rate of MIMO-UWB system for different material partitions and different antenna pairs at any outage probability. Based on the method, we can determine transmission rat of UWB system with and without MIMO in indoor environment by a given outage probability.

References

[1] Yang, L. and Giannakis, G. B., "Ultra-Wideband Communications: An Idea Whose Time Has Come," *IEEE Signal Processing Magazine*, Vol. 21, pp. 26–54 (2004).

[2] Roy, S., Foerster, J. R., Somayazulu, V. S. and Leeper, D. G., "Ultrawideband Radio Design: The Promise of High-Speed, Short-Range Wireless Connectivity," *Proceedings of the IEEE*, Vol. 92, pp. 295–311 (2004).

[3] "FCC Notice of Proposed Rule Making, Revision of Part 15 of the Commission's Rules Regarding Ultra-Wideband Transmission Systems," *Federal Communications Commission*, Washington, DC, ET-Docket 98-153 (2000).

[4] Abdulkareem Adinoyi and Halim Yanikomeroglu, "Practical Capacity Calculation for Time-Hopping Ultra-Wide Band Multiple-Access Communications," *IEEE Communications Letters*, Vol. 9, pp. 601–603 (2005).

[5] Tomaso Erseghe, "Capacity of UWB Impulse Radio with Single-User Reception in Gaussian Noise and Dense Multipath," *IEEE Trans. Communications*, Vol. 53, pp. 1257–1262 (2005).

[6] Fernando Ram´ırez-Mireles, "On the Capacity of UWB over Multipath Channels," *IEEE Communications Letters*, Vol. 9, pp. 523–525 (2005).

[7] Li, W., Gulliver, T. A. and Zhang, H., "Performance and Capacity of Ultra-Wideband Transmission with Biorthogonal Pulse Position Modulation over Multipath Fading Channels," *2005 IEEE International Conference*, pp. 225–229 (2005).

[8] Andrea Goldsmith, Syed Ali Jafar and Nihar Jindal, "Capacity Limits of MIMO Channels," *IEEE Journal on Selected Areas in Communications*, Vol. 21, pp. 684–702 (2003).

[9] Loyka, S. L., "Channel Capacity of MIMO Architecture Using the Exponential Correlation Matrix," *IEEE Communications Letters*, Vol. 5, pp. 369–371 (2001).

[10] Ziri-Castro, K. I., Scanlon, W. G. and Evans, N. E., "Prediction of Variation in MIMO Channel Capacity for the Populated Indoor Environment Using a Radar Cross-Section-Based Pedestrian Model," *IEEE Trans. Wireless Communications*, Vol. 4, pp. 1186–1194 (2005).

[11] Tang, Z. and Mohan, A. S., "Experimental Investigation of Indoor MIMO Ricean Channel Capacity," *IEEE Antennas and Wireless Propagation Letters*, Vol. 4, pp. 55–58 (2005).

[12] Browne, D. W., Majid Manteghi, Fitz, M. P. and Yahya Rahmat-Samii, "Experiments with Compact Antenna Arrays for MIMO Radio Communications," *IEEE Trans. Antennas and Propagation*, Vol. 54, pp. 3239–3250 (2006).

[13] Malik, W. Q., Mtumbuka, M. C., Edwards, D. J. and

Stevens, C. J., "Increasing MIMO Capacity in Ultra-Wideband Communications through Orthogonal Polarizations," *2005 IEEE 6th Workshop on Signal Processing Advances in Wireless Communications*, pp. 575–579 (2005).

[14] Zheng, F. and Thomas Kaiser, "On the Evaluation of Channel Capacity of Multi-Antenna UWB Indoor Wireless Systems," *ISSSTA2004*, pp. 525–529 (2004).

[15] Channel Modeling Sub-committee Report Final, *IEEE Std. p802.15-02/368r5-SG3a*, 18 November (2002).

[16] Zhao, Y., Hao, Y., Akram Alomainy and Clive Parini, "UWB On-Body Radio Channel Modeling Using Ray Theory and Subband FDTD Method," *IEEE Trans. Microwave Theory and Techniques*., Vol. 54, pp. 1827–1835 (2006).

[17] Zhang, Y. and Brown, A. K., "Complex Multipath Effects in UWB Communication Channels," *IEE Proc.-Commun*., Vol. 153, pp. 120–126 (2006).

[18] Richardson, P. C., Xiang, W. and Wayne Stark, "Modeling of Ultra-Wideband Channels within Vehicles," *IEEE Journal on Selected Areas in Communications*, Vol. 24, pp. 906–912 (2006).

[19] Driessen, P. F. and Foschini, G. J., "On the Capacity Formula for Multiple Input-Multiple Output Wireless Channels: A Geometric Interpretation," *IEEE Trans. Communications*, Vol. 47, pp. 173–176 (1999).

[20] Tila, F., Shepherd, P. R. and Pennock, S. R., "Theoretical Capacity Evaluation of Indoor Micro- and Macro-MIMO Systems at 5 GHz Using Site Specific Ray Tracing," *6th Electronics Letters*, Vol. 39, pp. 471–472 (2004).

[21] Oh, S. H. and Myung, N. H., "MIMO Channel Estimation Method Using Ray-Tracing Propagation Model," *14th Electronics Letters*, Vol. 40 (2004).

[22] Muqaibel, A., Safaai-Jazi, A., Bayram, A., Attiya, A. M. and Riad, S. M., "Ultrawideband Through-the-Wall Propagation," *IEE Proc.-Microw. Antennas Propag*., Vol. 152, pp. 581–588 (2005).

[23] Chen, S. H. and Jeng, S. K., "An SBR/Image Approach for Indoor Radio Propagation in a Corridor," *IEICE Trans. Electron*., Vol. E78-C, pp. 1058–1062 (1995).

[24] Chen, S. H. and Jeng, S. K., "SBR Image Approach for Radio Wave Propagation in Tunnels with and without Traffic," *IEEE Trans. Veh. Technol*., Vol. 45, pp. 570–578 (1996).

[25] Susana Loredo, Alberto Rodríguez-Alonso and Rafael P. Torres, "Indoor MIMO Channel Modeling by Rigorous GO/UTD-Based Ray Tracing," *IEEE Trans. Veh. Technol*., Vol. 57, pp. 680–692 (2008).

[26] Balanis, C. A., *Advanced Engineering Electromagnetics*, John Wiley & Sons (1989).

[27] Iskander, M. F. and Yun, Z., "Propagation Prediction Models for Wireless Communication Systems," *IEEE Trans. Microwave Theory and Technique*, Vol. 50, (2002).

[28] Malik, W. Q. and Edwards, D. J., "Measured MIMO Capacity and Diversity Gain with Spatial and Polar Arrays in Ultrawideband Channels," *IEEE Trans. Commun*., Vol. 55, pp. 2361–2370 (2007).

[29] Jakes, X. C., *Microwave Mobile Communication*, New York: Wiley (1974).

Manuscript Received: Apr. 21, 2009
Accepted: Dec. 31, 2009